Biotechnology for Biofuels

RESEARCH Open Access

Single mutation at a highly conserved region of chloramphenicol acetyltransferase enables isobutyl acetate production directly from cellulose by *Clostridium thermocellum* at elevated temperatures

Hyeongmin Seo[1,3†], Jong-Won Lee[2,3†], Sergio Garcia[1,3] and Cong T. Trinh[1,2,3*]

Abstract

Background: Esters are versatile chemicals and potential drop-in biofuels. To develop a sustainable production platform, microbial ester biosynthesis using alcohol acetyltransferases (AATs) has been studied for decades. Volatility of esters endows high-temperature fermentation with advantageous downstream product separation. However, due to the limited thermostability of AATs known, the ester biosynthesis has largely relied on use of mesophilic microbes. Therefore, developing thermostable AATs is important for ester production directly from lignocellulosic biomass by the thermophilic consolidated bioprocessing (CBP) microbes, e.g., *Clostridium thermocellum*.

Results: In this study, we engineered a thermostable chloramphenicol acetyltransferase from *Staphylococcus aureus* (CAT_{Sa}) for enhanced isobutyl acetate production at elevated temperatures. We first analyzed the broad alcohol substrate range of CAT_{Sa}. Then, we targeted a highly conserved region in the binding pocket of CAT_{Sa} for mutagenesis. The mutagenesis revealed that F97W significantly increased conversion of isobutanol to isobutyl acetate. Using CAT_{Sa} F97W, we demonstrated direct conversion of cellulose into isobutyl acetate by an engineered *C. thermocellum* at elevated temperatures.

Conclusions: This study highlights that CAT is a potential thermostable AAT that can be harnessed to develop the thermophilic CBP microbial platform for biosynthesis of designer bioesters directly from lignocellulosic biomass.

Keywords: Alcohol acetyltransferase, Thermostability, Chloramphenicol acetyltransferase, Isobutyl acetate, Esters, Consolidated bioprocessing, *Clostridium thermocellum*

Introduction

Esters are versatile chemicals that have been used as lubricants, solvents, food additives, fragrances, and potential drop-in fuels [1]. Currently, ester production largely relies on synthesis from petroleum or extraction from plants, which makes it neither sustainable nor economically feasible. Therefore, microbial production of esters has been studied for decades [2–7]. Most studies have employed an alcohol acetyltransferase (E.C. 2.3.1.84, AAT), belonging to a broad acetyltransferase class, that can synthesize a carboxylic ester by condensing an alcohol and an acyl-CoA in a thermodynamically favorable aqueous environment [5]. For example, an *Escherichia coli*, engineered to use this biosynthetic pathway, could achieve high titer of isobutyl acetate [6, 7]. With appropriate expression of AATs and availability of alcohol and acyl-CoA moieties, various types of esters can be produced [2, 4].

*Correspondence: ctrinh@utk.edu
†Hyeongmin Seo and Jong-Won Lee have contributed equally to this work
[1] Department of Chemical and Biomolecular Engineering, The University of Tennessee, Knoxville, TN, USA
Full list of author information is available at the end of the article

Due to high volatility of esters, ester production at elevated temperatures can benefit downstream product separation and hence reduce the process cost. Interestingly, it has recently been shown that for the same total carbon chain length, short-chain esters are less toxic to microbial health than alcohols, which is potentially beneficial for ester fermentation [8]. However, most of the AATs known to date are isolated from mesophilic microbes or plants [9–12], and none of them has been reported to be active at elevated temperatures (> 50 °C). The highest temperature reported for ester production is 42 °C in a thermotolerant yeast [13]. Hence, finding and developing a thermostable AAT are crucial to produce esters at elevated temperatures.

Chloramphenicol acetyltransferase (E.C. 2.3.1.28, CAT) is another acetyltransferase class that has been found in various microbes [14]. This enzyme acetylates chloramphenicol, a protein synthesis inhibitor, by transferring the acetyl group from acetyl-CoA. The acetylation of chloramphenicol detoxifies the antibiotic compound and confers chloramphenicol resistance in bacteria. Recent studies have implied that CATs likely recognize a broad substrate range for alcohols and acyl-CoAs [7]. In addition, high thermostability of some CATs enables them to be used as selection markers in thermophiles [15–17]. Therefore, CAT can function or be repurposed as a thermostable AAT suitable for ester biosynthesis at elevated temperatures.

In this study, we engineered a CAT from *Staphylococcus aureus* (CAT_{Sa}) for isobutyl acetate production at elevated temperatures. First, we investigated a broad alcohol substrate range of CAT_{Sa}. Protein homology modeling along with sequence alignment was performed to identify the binding pocket of CAT_{Sa} as a potential target for protein engineering to enhance condensation of isobutanol and acetyl-CoA. In silico mutagenesis discovered a variant (F97W) of CAT_{Sa} that was then experimentally validated for improved catalytic activity towards isobutanol. As a proof-of-concept, the engineered CAT_{Sa} was successfully expressed in *Clostridium thermocellum*. We further demonstrated a F97W CAT_{Sa}-overexpressing *C. thermocellum* for consolidated bioprocessing (CBP) to produce isobutyl acetate directly from cellulose without a need for external supply of cellulases. To our knowledge, this study presents the first demonstration of CAT engineering to enable ester production directly from cellulose at elevated temperatures.

Results and discussion

In silico and rapid in vivo characterization of a thermostable chloramphenicol acetyltransferase(s) for broad alcohol substrate range

To develop a thermophilic microbial ester production platform, a thermostable AAT is required. Unfortunately, the AATs known to date are isolated from mesophilic yeasts or plants [9–12], and none of them has been reported to be active at a temperature above 50 °C. To tackle this problem, we chose CATs to investigate their potential functions as a thermostable AAT, because some thermostable CATs have been successfully used as a selection marker in thermophiles [17–21] and others have been shown to perform the acetylation for not only chloramphenicol but various alcohols like AATs [7, 22–25] (Fig. 1a, Additional file 1: Figure S1A). As a proof-of-study, we investigated CAT_{Sa}, classified as Type A-9, from

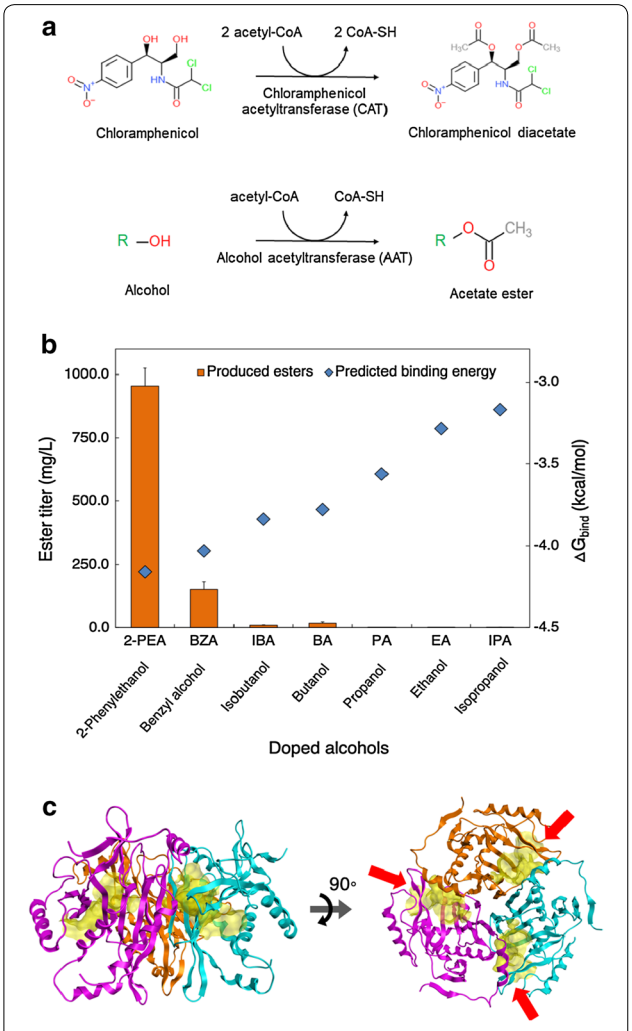

Fig. 1 Broad substrate specificity of CAT_{Sa}. **a** Acetylation of chloramphenicol and alcohol by a chloramphenicol acetyltransferase (CAT) and an alcohol acetyltransferase (AAT), respectively. **b** Comparison between the predicted binding free energies for various alcohols bound to the binding pocket of CAT_{Sa} and the titer of esters produced by an CAT_{Sa}-overexpressing *E. coli* with external supply of alcohols. **c** Structure of the CAT_{Sa} homology model. The red arrows indicate the binding pockets (in yellow cloud) formulated by the trimeric structure of CAT_{Sa}

the plasmid pNW33N for a broad range of alcohol substrates as it has been widely used for genetic engineering in *C. thermocellum* at elevated temperatures (≥ 50 °C) [17–19].

We first conducted alcohol docking simulations using the homology model. Remarkably, the model predicted binding affinities of short-to-medium-chain length alcohols (e.g., ethanol, propanol, isopropanol, butanol, and isobutanol) and aromatic alcohols (e.g., benzyl alcohol and phenethyl alcohol) to the binding pocket. The change in the protein's Gibbs free energy upon the substrate binding was ordered as follows: 2-phenethyl alcohol > benzyl alcohol > isobutanol > butanol > propanol > ethanol > isopropanol (Fig. 1b).

To quickly evaluate the in silico docking simulation results experimentally, we next performed in vivo characterization of a CAT_{Sa}-overexpressing *E. coli* and screened for acetate esters production. Acetyl-CoA was derived from glycolysis, while various alcohols were externally supplied to the medium. Remarkably, the results exhibited the same trend of specificities of CAT_{Sa} towards alcohols as predicted by the in silico docking simulation (Fig. 1b). The CAT_{Sa}-overexpressing *E. coli* produced all the expected acetate esters including ethyl acetate, propyl acetate, isopropyl acetate, butyl acetate, isobutyl acetate, benzyl acetate, and 2-phenethyl acetate at titers of 1.12 ± 0.07, 2.30 ± 0.28, 0.08 ± 0.02, 9.75 ± 1.57, 17.06 ± 6.04, 152.44 ± 29.50, and 955.27 ± 69.50 mg/L and specific ester production rates of 0.02 ± 0.00, 0.05 ± 0.01, 0.00 ± 0.00, 0.19 ± 0.03, 0.34 ± 0.12, 3.02 ± 0.57, and 19.27 ± 1.32 mg/gDCW/h, respectively. We observed that the specific ester production titers and rates are higher for aromatic alcohols than linear, short-chain alcohols likely because the hydrophobic-binding pocket of CAT_{Sa} has been evolved towards chloramphenicol [26], an aromatic antibiotic (Fig. 1c). Specifically, the bulky binding pocket of CAT_{Sa} likely contributes to more interaction with the aromatic substrates than the short, linear-chain alcohols (Additional file 1: Figure S1B, C).

Overall, thermostable CATs, e.g., CAT_{Sa}, can have broad range of substrate specificities towards linear, short-chain, and aromatic alcohols and hence can be harnessed as AATs for novel ester biosynthesis at elevated temperatures.

Discovery of a CAT_{Sa} variant improving conversion of isobutanol and acetyl-CoA into isobutyl acetate

Since the in vivo activity of CAT_{Sa} is more than 50-fold higher for the aromatic alcohols than isobutanol, we asked whether its activity could be improved for isobutyl acetate biosynthesis. Using the in silico analysis, we started by examining whether any modification of the binding pocket of CAT_{Sa} could improve the activity towards isobutanol. According to the homology model, the binding pocket consists of Tyr-20, Phe-27, Tyr-50, Thr-88, Ile-89, Phe-90, Phe-97, Ser-140, Leu-141, Ser-142, Ile-143, Ile-144, Pro-145, Trp-146, Phe-152, Leu-154, Ile-166, Ile-167, Thr-168, His-189, Asp-193, Gly-194, and Tyr-195, where the His189 and Asp193 are the catalytic sites (Fig. 2a). Since chloramphenicol resistance is likely a strong selective pressure throughout evolution, we expected all CATs to exhibit a common binding pocket structure. Unsurprisingly, conserved sequences in the binding pocket were observed by protein sequence alignment of CAT_{Sa} with other CATs of Type A (Additional file 1: Figure S2A). Especially, Pro-85 and Phe-97 were highly conserved in CATs of not only Type A but also Type B (Fig. 2b and Additional file 1: Figure S2B).

Based on the binding pocket identified, we performed docking simulation with alanine and residue scans using the acetyl-CoA–isobutanol–CAT_{Sa} complex to identify potential candidates for mutagenesis (Additional file 1: Figure S3A, B). Remarkably, the top three variant candidates were suggested at the Phe-97 residue (i.e., F97Y, F97W, and F97V). This residue is involved in the formation of a tunnel-like binding pocket [26]. Motivated by the analysis, Phe-97 was chosen for site-saturated mutagenesis, and the variants were screened in *E. coli* for isobutyl acetate production by external supply of isobutanol.

Among the variants characterized, the F97W variant exhibited the best performance (Fig. 2c), with the similar protein expression levels in *E. coli* (Additional file 1: Figure S4). As compared to the wild type, the F97W variant enhanced the isobutyl acetate production by fourfold. Subsequent in silico analysis showed that the mutation created a CH–π interaction between the hydrogen of isobutanol and the indole ring of F97W (Fig. 2d). The model also indicated no change in distance between the isobutanol and active site (His-189) in F97W. Therefore, the CH–π interaction is likely responsible for the improved activity of F97W variant towards isobutyl acetate biosynthesis.

In vitro characterization of CAT_{Sa} F97W

Before deploying CAT_{Sa} F97W for isobutyl acetate biosynthesis in the thermophilic CBP organism *C. thermocellum*, we checked whether the F97W mutation affected thermostability of the enzyme. We overexpressed and purified both the wild-type CAT_{Sa} and CAT_{Sa} F97W variant (Fig. 3a). The SDS-PAGE analysis confirmed the expression and purification of the enzymes by bands with the expected monomer size (25.8 kDa). Thermofluor assay revealed that the F97W variant slightly lowered the wild-type melting point from 72 to 68.3 °C (Fig. 3b). Since CAT_{Sa} F97W maintained high melting

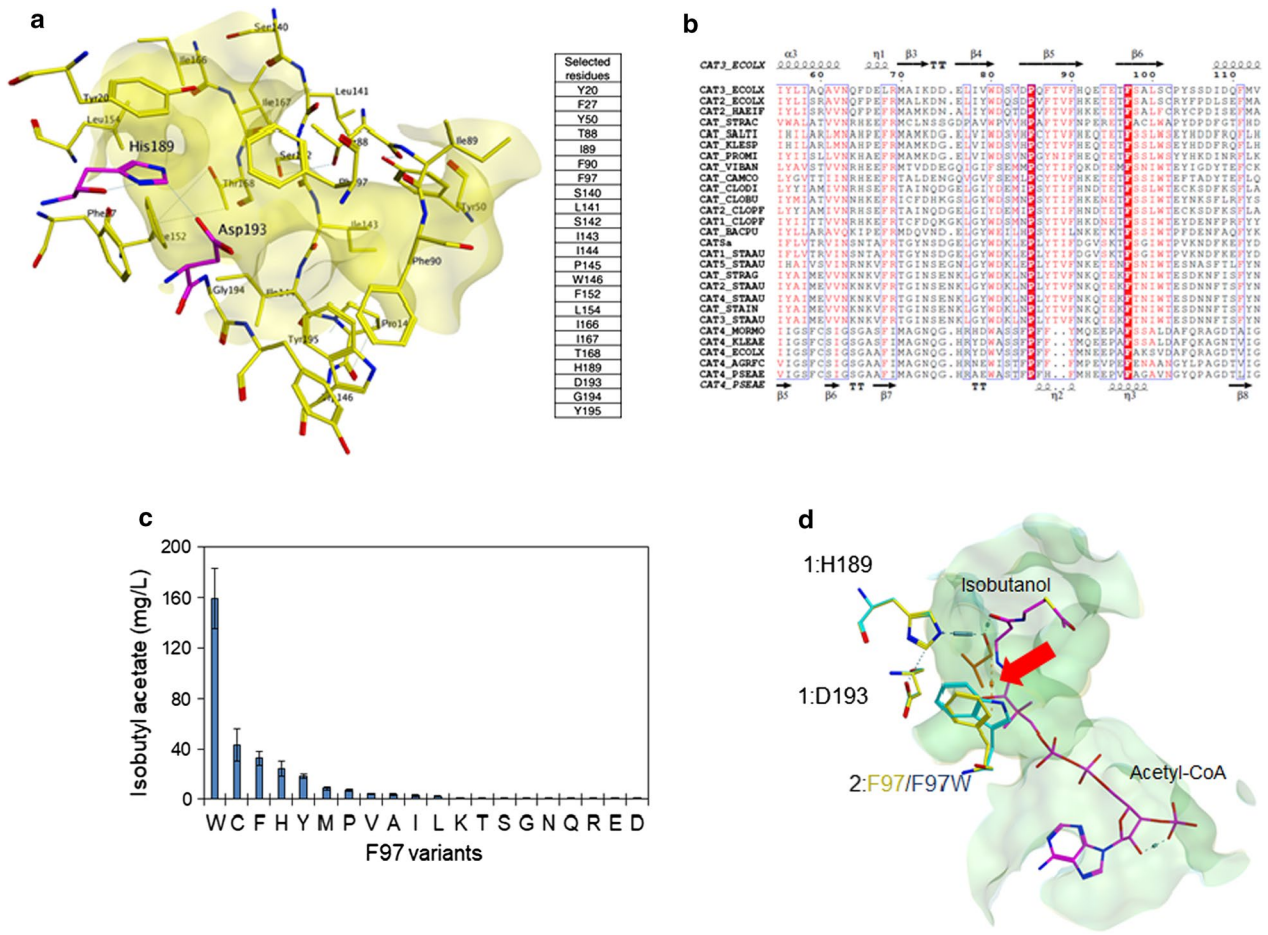

Fig. 2 Discovery of CAT_{Sa} F97W responsible for enhanced activity towards isobutanol. **a** A binding pocket of CAT_{Sa} and associated amino acid residues. The catalytic residues are in purple. **b** Protein sequence alignment of CAT_{Sa} with different CATs. **c** Screening of F97 variants for enhanced isobutyl acetate production in *E. coli*. The letters indicate amino acids substituting F in the wild-type CAT_{Sa}. **d** Superposed binding pocket structure of the wild-type and CAT_{Sa} F97W mutant. The red arrow indicates a CH–π interaction between the hydrogen of isobutanol and the indole ring of F97W

point, it is possible that CAT_{Sa} F97W still maintains its functionality at high temperature (≥ 50 °C), but needs to be thoroughly characterized.

Table 1 shows the in vitro enzymatic activities of both the wild-type CAT_{Sa} and CAT_{Sa} F97W at 50 °C. The turnover number (k_{cat}) of CAT_{Sa} F97W was two times higher than that of the wild type. The increased turnover number of CAT_{Sa} F97W led to 1.9-fold increase in enzymatic efficiency (k_{cat}/K_M, 4.08 ± 0.62, 1/M/s), while the mutation did not result in significant change in K_M. The improved enzymatic efficiency of CAT_{Sa} F97W agrees with the enhanced isobutanol production observed in the in vivo characterization using the CAT_{Sa}-overexpressing *E. coli* (Fig. 2c).

Based on the rigidity of the binding pocket, we originally presumed that mutagenesis on the binding pocket would result in activity loss towards chloramphenicol. Surprisingly, CAT_{Sa} F97W retained the activity towards chloramphenicol (Table 1). The F97W mutation decreased k_{cat}, but also lowered K_M, resulting in a compensation effect. Turnover number of CAT_{Sa} (k_{cat}, 202.97 ± 3.36, 1/s) was similar to the previously reported value by Kobayashi et al. [16], but K_M (0.28 ± 0.02, mM) was about 1.75-fold higher. The difference might attribute to the experimental condition and analysis performed. Kobayashi et al. used chloramphenicol in a range of 0.05–0.2 mM for the assay and the Lineweaver–Burk method for analysis, while we used a 0–1.0 mM range with a non-linear regression analysis method. Interestingly, affinity towards acetyl-CoA was independent of the alcohol co-substrates (Additional file 1: Table S2), suggesting that the alcohol affinity would be likely the main bottleneck for microbial production of isobutyl acetate.

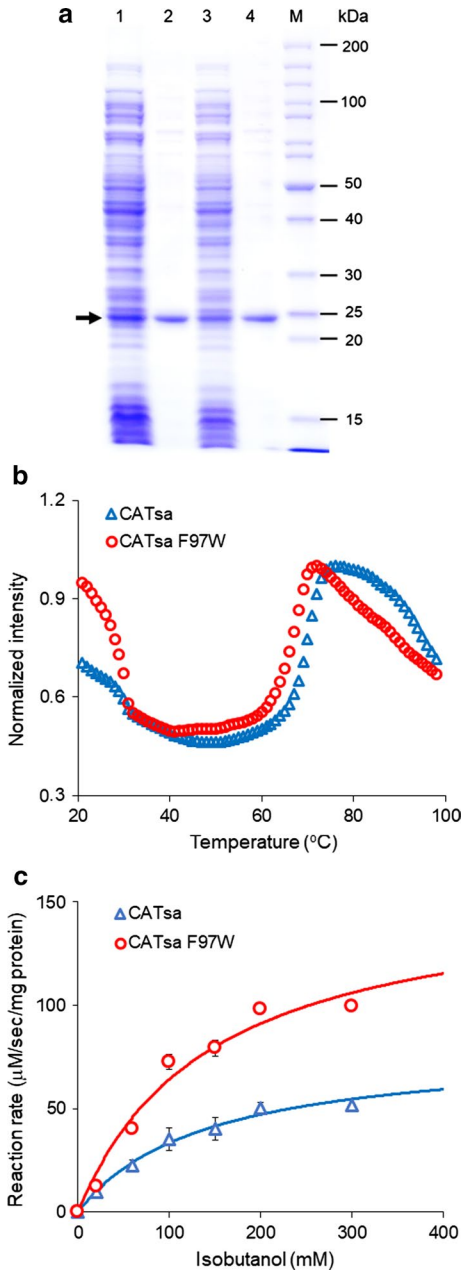

Fig. 3 In vitro characterization of the wild-type CAT_{Sa} and CAT_{Sa} F97W variant. **a** SDS-PAGE of the purified CAT_{Sa} and CAT_{Sa} F97W. The black arrow indicates the expected size of expressed target proteins, including CAT_{Sa} and CAT_{Sa} F97W. Notations: column 1, crude cell extract of IPTG induced *E. coli* BL21(DE3) harboring pET_CAT$_{Sa}$; column 2, His-tag purified CAT_{Sa}; column 3, crude extract of IPTG induced *E. coli* BL21(DE3) harboring pET_ CAT_{Sa} F97W; column 4, His-tag purified CAT_{Sa} F97W; and M, protein ladder. **b** Melting curve of CAT_{Sa} and CAT_{Sa} F97W. The intensity was normalized by each maximum value. **c** Michaelis–Menten plots of CAT_{Sa} and CAT_{Sa} F97W for various isobutanol concentrations at 50 °C. The co-substrate, acetyl-CoA, was supplemented at the saturated concentration of 2 mM. The error bars represent standard deviation of three biological replicates

Taken altogether, the F97W mutation not only resulted in 1.9-fold higher enzymatic efficiency towards isobutanol but also retained thermostability of CAT_{Sa}. Thus, CAT_{Sa} F97W variant can serve a starting candidate to demonstrate direct biosynthesis of isobutyl acetate at elevated temperatures by *C. thermocellum*.

Isobutyl acetate production from cellulose at elevated temperatures by an engineered *C. thermocellum* overexpressing CAT_{Sa} F97W

We next investigated whether *C. thermocellum* overexpressing CAT_{Sa} F97W could produce isobutyl acetate at elevated temperatures. This thermophile was chosen, because it has a high cellulolytic activity suitable for CBP, a one-step process configuration for cellulase production, cellulose hydrolysis, and fermentation for direct conversion of lignocellulosic biomass to fuels and chemicals [27]. Furthermore, studies have demonstrated that the wild-type *C. thermocellum* has native metabolism capable of endogenously producing precursor metabolites for ester biosynthesis, such as acetyl-CoA, isobutyryl-CoA, as well as ethanol [28] and higher alcohols (e.g., isobutanol) under high cellulose loading fermentation [29–31] (Fig. 4a, Additional file 1: Figure S5A).

We started by generating two isobutyl acetate-producing strains, HSCT0101 and HSCT0102, by introducing the plasmids pHS0024 (harboring the wild-type CAT_{Sa}) and pHS0024_F97W (harboring the CAT_{Sa} F97W variant) into *C. thermocellum* DSM1313. Colonies were isolated on antibiotic-selective plates at 55 °C. Successful transformation clearly indicated that CAT_{Sa} F97W conferred the thiamphenicol resistance and hence maintained CAT activity. This result agrees with the in vitro enzymatic activity of CAT_{Sa} F97W (Table 1).

We next evaluated whether the *C. thermocellum* strains could synthesize isobutyl acetate from cellobiose. Since the endogenous isobutanol production from a typical cellobiose concentration (5 g/L) is low [31], we supplemented the medium with 2 g/L isobutanol. Both HSCT0101 and HSCT0102 could produce isobutyl acetate at 55 °C as expected. Like the in vivo characterization in *E. coli* (Fig. 2c), HSCT0102 outperformed HSCT0101 with 3.5-fold increase in isobutyl acetate production (Fig. 4b). Interestingly, we also observed the parent *C. thermocellum* M1354 produced a trace amount of isobutyl acetate (< 0.1 mg/L), even though this strain does not harbor a CAT (Additional file 1: Figure S5). This phenomenon was only observed when hexadecane overlay was used during fermentation for ester extraction. One possible explanation is the endogenous activity of esterases in *C. thermocellum* might have been responsible for low isobutyl acetate production, while the organic phase overlay

Table 1 Kinetic parameters of the wild-type CAT_{Sa} and mutant CAT_{Sa} F97W

Substrates	CAT_{Sa}		CAT_{Sa} F97W	
	Chloramphenicol	Isobutanol	Chloramphenicol	Isobutanol
K_M (mM)	0.28 ± 0.02	138.66 ± 28.92	0.18 ± 0.01	144.77 ± 23.65
k_{cat} (1/s)	202.97 ± 3.36	0.30 ± 0.03	102.63 ± 2.04	0.59 ± 0.05
k_{cat}/K_M (1/M/s)	7.37 ± 0.48 × 10^5	2.16 ± 0.45	5.77 ± 0.49 × 10^5	4.08 ± 0.62

The reactions were performed at 50 °C. The co-substrate, acetyl-CoA, was supplied at the saturated concentration of 2 mM. Melting temperature (Tm) of CAT_{Sa} and CAT_{Sa} F97W is 72.0 ± 0.8 and 68.3 ± 1.2 °C, respectively

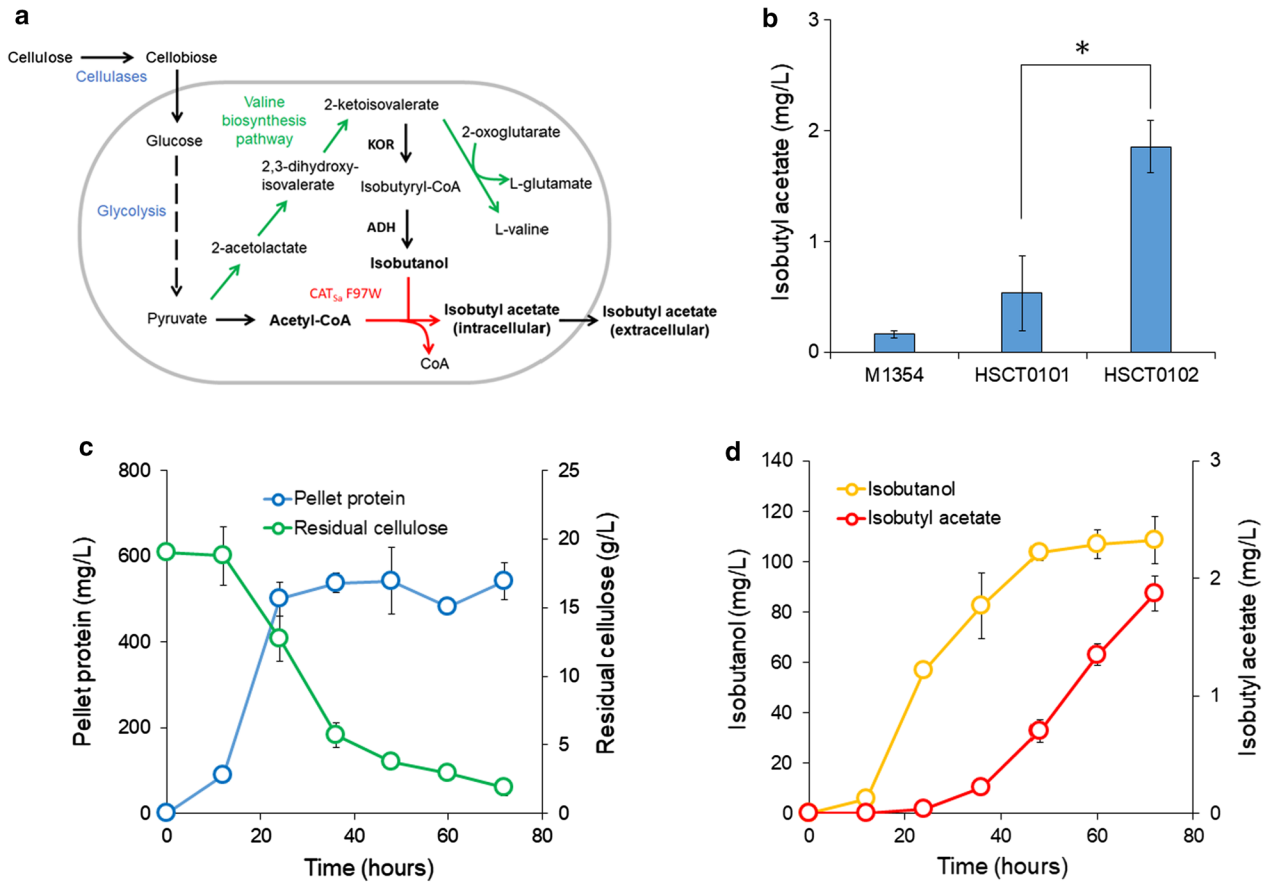

Fig. 4 Isobutyl acetate production in the engineered *C. thermocellum*. **a** A simplified isobutyl acetate production pathway from cellulose in *C. thermocellum*. **b** Biosynthesis of isobutyl acetate of the wild-type and engineered *C. thermocellum* strains at 55 °C from MTC medium with 5 g/L cellobiose and external supply of 2 g/L isobutanol. Isobutyl acetate was measured after 24 h from the hexadecane layer of cell cultures. Initial OD of each cell culture was in a range of 0.8–1.0. The error bars represent standard deviation of five biological replicates. Statistical analysis: *t* test, "*" *p* value < 4 × 10^{-4}, $t = -6.475$, $df = 7$. **c** Kinetic profiles of cell growth and residual cellulose of HSCT0102. HSCT0102 was cultured in C-MTC medium with 20 g/L Avicel PH-101. The error bars represent standard deviation of three biological replicates. **d** Kinetic profiles of isobutanol and isobutyl acetate production by HSCT0102 in C-MTC medium with 20 g/L Avicel PH-101. The error bars represent standard deviation of three biological replicates. *KOR* 2-ketoisovalerate ferredoxin oxidoreductase, *ADH* alcohol dehydrogenase

helps to extract the target ester. It should be noted that the esterase reaction is reversible and more thermodynamically favorable for ester degradation than biosynthesis.

Finally, we tested whether HSCT0102 could endogenously produce isobutyl acetate directly from cellulose at elevated temperatures (55 °C). After 72 h, cell mass, containing 550 mg/L of pellet protein, reached 1.04 g/L, and 17 g/L of cellulose were consumed (Fig. 4c). About 103 mg/L of isobutanol were produced for the first 48 h and further increased up to 110 mg/L for additional 24 h

(Fig. 4d). Besides isobutanol, *C. thermocellum* also produced other fermentative metabolites, including ethanol, formate, acetate, and lactate, as expected (Additional file 1: Figure S6A, B). For the target isobutyl acetate production, HSCT0102 did not produce isobutyl acetate for the first 24 h but started accumulating the target product for the next 48 h. The observed profile of isobutyl acetate production could be attributed to the low substrate affinity of CAT_{Sa} F97W (Table 1). The final titer of isobutyl acetate reached 1.9 mg/L.

Besides isobutyl acetate, we also observed that HSCT0102 produced other detectable esters such as ethyl acetate, ethyl isobutyrate, and isobutyl isobutyrate (Additional file 1: Figure S6A, C, D). Endogenous biosynthesis of these esters could be explained from the complex redox and fermentative metabolism of *C. thermocellum* [30, 32]. Specifically, *C. thermocellum* can endogenously synthesize the precursor metabolites, acetyl-CoA and ethanol via the ethanol biosynthesis pathway, as well as isobutyryl-CoA and isobutanol via the valine biosynthesis pathway (Additional file 1: Figure S6A). With the availability of these four precursor metabolites, *C. thermocellum* could make ethyl acetate, ethyl isobutyrate, isobutyl acetate, and isobutyl isobutyrate as observed experimentally (Additional file 1: Figure S6C, D).

Taken altogether, *C. thermocellum* overexpressing CAT_{Sa} F97W successfully produced the target isobutyl acetate from cellulose at elevated temperatures (55 °C). However, the low titer and conversion rate require optimization to improve isobutyl acetate production in future studies. One of the key metabolic engineering targets is to enhance enzymatic efficiency of CAT_{Sa}. In contrast to *S. cerevisiae*-derived ATF1 that has high specificity towards isobutanol [6] and can be expressed in *E. coli* to achieve a high titer of 17.5 g/L isobutyl acetate and 80% theoretical maximum product yield [7], CAT_{Sa} F97W exhibits a relatively low affinity towards isobutanol. The rationale for utilizing CAT_{Sa} instead of ATF1 is that CAT_{Sa} is thermostable, and this study is the first ever to report its function for ester production at elevated temperatures. Tuning gene expression in *C. thermocellum* is another challenge that needs to be addressed for enhanced ester production. Since CAT_{Sa} F97W still retains the activity towards chloramphenicol, adaptive evolution strategies such as chemically induced chromosomal evolution (CIChE) can offer a promising strategy to improve the gene expression level [33]. Finally, model-guided optimization at system levels should be implemented for the most effective conversion of cellulose into isobutyl acetate to achieve high production of isobutyl esters and other class of esters [34–36].

Conclusions

This study demonstrated that a CAT can function and/or be repurposed as an AAT for novel biosynthesis of designer esters at elevated temperatures. Both in silico and in vivo characterization discovered a broad alcohol substrate range of the thermostable chloramphenicol acetyltransferase from *S. aureus* (CAT_{Sa}). Discovery of the F97W mutation of CAT_{Sa} by model-guided protein engineering enhanced isobutyl acetate production. This study presented the consolidated bioprocessing of cellulose into ester(s) by the thermophilic CBP organism *C. thermocellum* harboring an engineered thermostable CAT_{Sa} F97W. Overall, this research helps to establish a foundation for engineering non-model organisms for direct conversion of lignocellulosic biomass into designer bioesters.

Materials and methods

Bacterial strains and plasmids

Bacterial strains and plasmids used in this study are listed in Table 2. *Clostridium thermocellum* DSM1313 Δ*hpt* (M1354) strain was used as a host for the ester production at elevated temperatures. It should be noted that the deletion of hypoxanthine phosphoribosyltransferase gene (*hpt*, Clo1313_2927) in the wild-type DSM1313 allows genetic engineering by 8-azahypoxanthine (8-AZH) counter selection; this deletion does not have any known adverse effect on cell growth and metabolism [37, 38]. The plasmid pNW33N, containing CAT_{Sa}, is thermostable and was used to express various CATs in *C. thermocellum*. The pET plasmids were used for molecular cloning and enzyme expression in *E. coli*.

Chemicals and reagents

All chemicals were purchased from Sigma-Aldrich (MO, USA) and/or Thermo Fisher Scientific (MA, USA), unless specified elsewhere. For molecular cloning, restriction enzymes and T4 ligase were obtained from New England Biolabs (MA, USA). Phusion Hot Start II DNA polymerase was used for polymerase chain reaction (PCR).

Media and cultivation

For molecular cloning and protein expression, *E. coli* strains were grown in lysogeny broth (LB) containing appropriate antibiotics unless noted otherwise. For in vivo characterization of CAT_{Sa} in *E. coli*, M9 hybrid medium [5] with 20 g/L glucose was used. For *C. thermocellum* culture, MTC minimal medium or CTFuD-NY medium [38] was used as specified in the experiments.

Table 2 Plasmids and strains used in this study

Name	Descriptions	Source
Plasmids		
pNW33N	*Bacillus–E. coli* shuttle vector, Cm^R, pBC1 ori for Gram-positive strains, pBR322 ori for *E. coli*, source of CAT_{Sa}	Bacillus Genetic Stock Center
pETDuet-1	pBR322 ori, Amp^R, lacI, T7lac promoter	Novagen
pET_CAT_{Sa}	CAT_{Sa} wild-type encoding gene between *Bam*HI, *Sac*I site, pETDuet-1 backbone, 6× His-tag at N-terminus	This study
pET_CAT_{Sa} F97W	F97W site-directed variant, pET_CAT_{Sa} backbone	This study
pHS0024	CAT_{Sa} wild-type gene under *C. thermocellum* PgapDH promoter, downstream of Clo1313_2927 for the transcription terminator, tdk operon under cbp promoter substituting with the native cat selection marker, pNW33N plasmid backbone	This study
pHS0024_F97W	CAT_{Sa} F97W site-directed mutated from pHS0024	This study
Strains		
E. coli Top10	Host for molecular cloning, *mcrA*, *Δ(mrr-hsdRMS-mcrBC)*, *Phi80lacZ(del)M15*, *ΔlacX74*, *deoR*, *recA1*, *araD139*, *Δ(ara-leu)7697*, *galU*, *galK*, *rpsL(SmR)*, *endA1*, *nupG*	Invitrogen
E. coli BL21 (DE3)	*E. coli* B *dcm*, *ompT*, *hsdS*(rB-mB-), *gal*	Invitrogen
M1354	*C. thermocellum* DSM1313 *Δhpt*	[37]
HSCT0101	M1354 harboring pHS0024	This study
HSCT0102	M1354 harboring pHS0024_F97W	This study

The plasmids containing mutagenized genes are presented in Additional file 1: Table S1

Optical density (OD) was measured by a spectrophotometer at 600 nm wavelength (Spectronic 200+, Thermo Fisher Scientific, MA, USA).

Multiple sequence alignment analysis

Multiple sequence alignment (MSA) analysis was performed using MEGA7 [39]. Protein sequences were aligned by ClustalW [40] and visualized by ESPript 3.0 (http://espript.ibcp.fr) [41]. The key features in protein structures of 3U9F [42], 4CLA [43], and 2XAT [44] were extracted from CAT_SALTI, CAT3_ECOLIX, and CAT4_PSEAE, respectively.

Molecular modeling and docking simulations

Three-dimensional (3D) structures

The 3D structure of CAT_{Sa} and alcohols of interest was first generated using Swiss-Model [45] and the 'Builder' tools of MOE (Molecular Operating Environment software, version 2019.01), respectively. The 3D structure of the dual substrate-bounded CAT_{Sa} complex (i.e., acetyl-CoA–isobutanol–CAT_{Sa}) was obtained by extracting an isobutanol from the isobutanol–CAT_{Sa} complex and then adding it to the acetyl-CoA–CAT_{Sa} complex. All the structures were prepared by the 'QuickPrep' tool of MOE with default parameters and further optimized by energy minimization with the Amber10:EHT force field.

Docking simulation

To perform docking simulations, the potential binding pocket was searched using the 'Site Finder' tool of MOE. The best-scored site, consistent with the reported catalytic sites [46], was selected for further studies. Docking simulations were performed as previously described [47]. Briefly, acetyl-CoA and each alcohol were docked using the induced fit protocol with the Triangle Matcher placement method and the London ΔG scoring function. After the docking simulations, the best-scored binding pose, showing the crucial interaction between the residue and the substrate at root-mean-square-deviation (RMSD) < 2 Å, was selected. As an example, for the acetyl-CoA docking, the binding pose exhibiting the hydrogen bond between the hydroxyl of Ser-148 and the N^{71} of the CoA was chosen [48]. For the alcohol docking, the binding pose showing the hydrogen bond between the N^3 of His-189 and the hydroxyl of alcohol was selected [26].

In silico mutagenesis analysis

In silico mutagenesis analysis of the acetyl-CoA–isobutanol–CAT_{Sa} complex was carried out as previously described [47]. Specifically, the 'alanine scan' and 'residue scan' tools of MOE were used to identify the potential residue candidates for mutagenesis.

Molecular cloning

Plasmid construction

Plasmids were constructed by the standard molecular cloning technique of ligase dependent method and/or Gibson assembly [49] using the primers listed in Additional file 1: Table S1. The constructed plasmids were

introduced into *E. coli* TOP10 by heat shock transformation. Colonies isolated on a selective plate were PCR screened and plasmid purified. The purified plasmids were verified via Sanger sequencing before being transformed into *E. coli* BL21 (DE3). Site-directed mutagenesis was performed using the QuickChange™ site-directed mutagenesis protocol with reduced overlap length [50] or Gibson assembly method [49]. For the *C. thermocellum* engineering, the plasmid pHS005 was constructed first and then modified to pHS0024. pHS0024 has no *hpt* at the downstream of the operon, while other sequences of the plasmid are identical to pHS005.

Transformation

The conventional chemical transformation and electroporation methods were used for transformation of *E. coli* [51] and *C. thermocellum* [38], respectively. For *C. thermocellum*, the method, however, was slightly modified as described here. First, *C. thermocellum* M1354 (Table 2) was cultured in 50 mL CTFuD-NY medium at 50 °C inside an anaerobic chamber (Bactron300, Sheldon manufacturing Inc., OR, USA). The cell culture with OD in a range of 0.8–1.0 was cooled down at room temperature for 20 min. Beyond this point, all steps were performed outside the chamber. The cooled cells were harvested at 6500×*g* and 4 °C for 20 min. The cell pellets were washed twice with ice-chilled Milli-Q water and resuspended in 200 µL of the transformation buffer consisting of 250 mM sucrose and 10% (v/v) glycerol. Several 30 µL aliquots of the electrocompetent cells were immediately stored at −80 °C for further use. For electroporation, the electrocompetent cells were thawed on ice and incubated with 500–1000 ng of methylated plasmids [52] for 10 min. Then, the cells were transferred to an ice-chilled 1-mm gap electroporation cuvette (BTX Harvard Apparatus, MA, USA) followed by two consecutive exponential decay pulses with 1.8 kV, 350 Ω, and 25 µF. The pulses usually resulted in a 7.0–8.0 ms time constant. The cells were immediately resuspended in prewarmed fresh CTFuD-NY and recovered at 50 °C under anaerobic condition (90% N_2, 5% H_2, and 5% CO_2) inside a rubber capped Balch tube. After 0–12 h of recovery, the cells were mixed with molten CTFuD-NY agar medium supplemented with 15 µg/mL thiamphenicol. Finally, the medium-cell mixture was poured on a petri dish and solidified inside the anaerobic chamber. The plate was incubated at 50 °C up to 1 week until colonies appeared. Transformation efficiency was 2–100 colony-forming units per µg plasmid (CFU/µg plasmid).

In vivo characterization of CAT_{Sa} and its variants in *E. coli*

For in vivo characterization of CAT_{Sa} and its variants in *E. coli*, high-cell density cultures were performed as previously described [53] with an addition of 2 g/L of various alcohols. For in situ extraction of esters, each tube was overlaid with 25% (v/v) hexadecane. To confirm the protein expression of CAT_{Sa} and its variants, 1% (v/v) of stock cells were grown overnight at 37 °C and 200 rpm in 15 mL culture tubes containing 5 mL of LB medium and antibiotic. Then, 4% (v/v) of the overnight cultures were transferred into 1 mL of LB medium containing antibiotic in a 24-well microplate. The cultures were grown at 37 °C and 350 rpm using an incubating microplate shaker (Fisher Scientific, PA, USA) until OD reached to 0.4–0.6 and then induced by 0.1 mM isopropyl β-D-1-thiogalactopyranoside (IPTG) for 4 h with a Breathe-Easy Sealing Membrane to prevent evaporation and cross contamination (cat# 50-550-304, Research Products International Corp., IL, USA). The protein samples were obtained using the B-PER complete reagent (cat# 89822, Thermo Scientific, MA, USA), according to the manufacturer's instruction and analyzed by SDS-PAGE.

Enzyme characterization

His-tag purification

For enzyme expression, an overnight culture was inoculated with a 1:50 ratio in fresh LB medium containing 1 mM IPTG and antibiotic, followed by 18 °C overnight incubation (up to 20 h) in a shaking incubator at 200 rpm. The induced cells were harvested by centrifugation at 4 °C, and 4700×*g* for 10 min. The cell pellet was then washed once with Millipore water and resuspended in the B-PER complete reagent. After 30 min incubation at room temperature, the mixture was centrifuged at 17,000×*g* for 2 min. The supernatant was collected and designated as crude extract. For His-tag purification, the crude extract was incubated with HisPur Ni–NTA superflow agarose in a batch as the manufacturer recommends. Then, the resin was washed with at least three volumes of wash buffer, consisting of 50 mM Tris–HCl (pH 8.0), 300 mM NaCl, 10 mM imidazole, and 0.1 mM EDTA. The resin bound proteins were eluted by 300 µL elution buffer containing 50 mM Tris–HCl (pH 8.0), 50 mM NaCl, 300 mM imidazole, and 0.1 mM EDTA. The eluted sample was then desalted and concentrated via an Amicon filter column with 10 kDa molecular weight cut-off. Finally, the protein sample was suspended in 200 µL of 20 mM Tris–HCl buffer (pH 8.0). Protein concentration was measured by the Bradford assay [54] with bovine serum albumin (BSA) as the reference protein.

Thermal shift assay

To measure protein melting temperature (Tm), a thermofluor assay was employed with SYPRO Orange [55]. About 10–250 µg of His-tag purified protein was mixed with 5× SYPRO Orange in a 50 µL final volume in a

96-well qPCR plate. The plate was sealed with PCR caps before running the assay. The StepOne real-time PCR machine (Applied Biosystems, CA, USA) was used to run the assay with the following parameters: ROX reporter, 1 °C increment per cycle, 1-min hold at every cycle, and temperature range from 20 to 98 °C. The data were collected, exported, and processed to calculate Tm.

5,5′-dithiobis-(2-nitrobenzoic acid) (DTNB) assay

Reaction rate for each CAT was determined by a DTNB assay [56] in a 384-well plate. Total reaction volume was 50 µL with the reaction buffer comprising of 50 mM Tris–HCl (pH 8.0). Concentrations of acetyl-CoA (CoALA Biosciences, TX, USA) and alcohols were varied as specified in each experiment. Final enzyme concentrations of 0.05 µg/mL and 10 µg/mL were used for the reactions towards chloramphenicol and alcohols, respectively. Reaction kinetics was collected by measuring absorbance at 412 nm every minute for 1 h at 50 °C in a microplate reader (Synergy HTX microplate reader, BioTek). The reaction rate was calculated using the extinction coefficient from a standard curve of free coenzyme A (MP Biomedicals, OH, USA) under the same condition. It should be noted that since the maximum operating temperature recommended for the plate reader is 50 °C, the high-throughput enzyme assay for CAT at elevated temperatures was only performed to determine enzyme kinetics parameters.

Calculation of kinetic parameters for reaction rates

The parameters of Michaelis–Menten rate law (Eq. 1) were calculated for each enzyme as follows. First, linear regression was performed on data collected from a microplate reader to identify initial reaction rates, y_i, at different initial substrate concentrations, s_i, where $i = \{1,2,\ldots,n\}$ is the number of data points collected. Then, these initial reaction rates and associated initial substrate concentrations for all replicates were simultaneously fit to the Michaelis–Menten model (Eq. 1) using robust non-linear regression (Eq. 2) with a soft-L1-loss estimator (Eq. 3) as implemented in the SciPy numerical computing library v1.2.0 [57, 58]:

$$v_i = \frac{v_{\max} s_i}{K_M + s_i} \tag{1}$$

$$\min_{k_m, v_{\max}} \sum_{i=1}^{n} \rho\left(\left(v_i(s_i, K_M, v_{\max}) - y_i\right)^2\right) \tag{2}$$

$$\rho(z) = 2\left(\sqrt{1+z}\right) - 1. \tag{3}$$

The least-squares problem determines the parameters K_M and $v_{\max}$ by minimizing the difference between the model predicted reaction rates v_i and measured reaction rates y_i (Eq. 2). A smoothing function $\rho(z)$ is used to make the least square problem resistant to outliers (Eq. 3). Due to the unbiased resistance to outliers and the avoidance of errors resulting from conventional linearization methods, robust non-linear regression provides the most precise parameter estimate for the Michaelis–Menten model [59].

Isobutyl acetate production in *C. thermocellum*

Cellobiose fermentation

Isobutyl acetate production from cellobiose in *C. thermocellum* strains was performed by the two-step bioconversion configuration. Cells were first cultured in MTC minimal medium [38] containing 5 g/L cellobiose in a rubber capped Balch tube until OD reached 0.8–1.0. The cells were cooled down at room temperature for 20 min and centrifuged at 4700×*g* and 4 °C for 20 min. After removing the supernatant, cells were resuspended in the same volume of fresh MTC minimal medium containing 2 g/L isobutanol in an anaerobic chamber. The cell suspension was then divided into 800 µL in a 2.0 mL screw cap microcentrifuge tube with a 200 µL hexadecane overlay. The cells were incubated at 55 °C for 24 h followed by analysis of gas chromatography coupled with a mass spectrometer (GC/MS) to quantify the amount of isobutyl acetate produced.

Cellulose fermentation

For the cellulose fermentation, modified MTC medium (C-MTC medium) was used. 20 g/L of Avicel PH-101 was used as a sole carbon source instead of cellobiose, and 10 g/L of MOPS was added to increase buffer capacity. Initial pH was adjusted to 7.5 by 5 M KOH and autoclaved. In an anaerobic chamber, 0.8 mL of overnight cell culture was inoculated in 15.2 mL of C-MTC medium (1:20 inoculation ratio) with 4 mL of overlaid hexadecane. Each tube contained a small magnetic stirrer bar to homogenize cellulose. The rubber capped Balch tube was incubated in a water bath connected with a temperature controller set at 55 °C and a magnetic stirring system. Following pH adjustment with 70 µL of 5 M KOH injection, 800 µL of cell culture and 200 µL of hexadecane layer were sampled every 12 h. Culture pH was maintained within a range of 6.4–7.8 during the fermentation.

Cell growth was monitored by measuring pellet protein. The cell–cellulose pellet from 800 µL sampling volumes was washed twice with Milli-Q water and suspended by 200 µL lysis buffer (0.2 M NaOH, 1% SDS) followed by an hour incubation at room temperature. Then, the solution was neutralized with 50 µL 0.8 M HCl and

diluted by 550 µL water. The mixture was centrifuged at 17,000×*g* for 3 min. Protein concentration from the supernatant was analyzed by the detergent-compatible Bradford assay (Thermo Scientific, WA, USA). The residual pellet was boiled in a 98 °C oven for an hour before quantifying residual cellulose.

Residual cellulose was quantified by the phenol–sulfuric acid method [60] with some modifications. The boiled sample was washed twice with Milli-Q water and suspended in 800 µL water to make equivalent volume to the original. The sample was homogenized by pipetting and vortexing for 10 s, and 20 µL of the homogenized sample was transferred to a new 2.0 mL microcentrifuge tube or 96-well plate and dried overnight in a 55 °C oven. The dried pellet was suspended in 200 µL of 95% sulfuric acid and incubated for an hour at room temperature. After the pellet was dissolved completely, 20 µL of 5% phenol was added and mixed with the sulfuric acid solution. After 30 min incubation at room temperature, 100 µL of the sample was transferred to a new 96-well plate, and the absorbance at 490 nm was measured. The absorbance was converted to cellulose concentration by the standard curve of Avicel PH-101 treated by the same procedure.

Analytical methods

High-performance liquid chromatography (HPLC)

Extracellular metabolites were quantified using a high-performance liquid chromatography (HPLC) system (Shimadzu Inc., MD, USA). 800 µL of culture samples was centrifuged at 17,000×g for 3 min, and then, the supernatants were filtered through 0.2 µm filters and run with 10 mN H_2SO_4 mobile phase at 0.6 mL/min on an Aminex HPX-87H (Biorad Inc., CA, USA) column at 50 °C. Refractive index detector (RID) and ultra-violet detector (UVD) at 220 nm were used to monitor concentrations of sugars, organic acids, and alcohols.

Gas chromatography coupled with mass spectroscopy (GC/MS)

Esters were measured by GC (HP 6890, Agilent, CA, USA) equipped with an MS (HP 5973, Agilent, CA, USA). For the GC system, the Zebron ZB-5 (Phenomenex, CA, USA) capillary column (30 m × 0.25 mm × 0.25 µm) was used to separate analytes, and helium was used as the carrier with a flow rate of 0.5 mL/min. The oven temperature program was set as follows: 50 °C initial temperature, 1 °C/min ramp up to 58 °C, 25 °C/min ramp up to 235 °C, 50 °C/min ramp up to 300 °C, and 2-min bake-out at 300 °C. 1 µL of sampled hexadecane layer was injected into the column in the splitless mode with an injector temperature of 280 °C. For the MS system, selected ion mode (SIM) was used to detect and quantify esters with the following parameters: (i) ethyl acetate, *m*/*z* 45.00 and 61.00 from 4.2 to 4.6 min retention time (RT), (ii) isopropyl acetate, *m*/*z* 45 and 102 from 4.7 to 5.0 min RT, (iii) propyl acetate, *m*/*z* 59 and 73 from 5.2 to 5.8 min RT, (iv) ethyl isobutyrate, *m*/*z* 73 and 116 from 6.1 to 6.6 min RT, (v) isobutyl acetate, *m*/*z* 61 and 101 from 6.6 to 7.6 min RT, (vi) butyl acetate, *m*/*z* 61 and 116 from 7.7 to 9.2 min RT, (vii) isobutyl isobutyrate, *m*/*z* 89 and 129 from 10.1 to 12.5 min RT, (viii) benzyl acetate, *m*/*z* 108 and 150 from 13.1 to 13.8 min RT, and (ix) 2-phenethyl acetate, *m*/*z* 104 and 121 from 13.8 to 15.5 min RT. Isoamyl alcohol and isoamyl acetate were used as the internal standard analytes. The esters were identified by RT and quantified by the peak areas and standard curves. Standard curves were determined using pure esters diluted into hexadecane at concentrations of 0.01 g/L, 0.05 g/L, 0.1 g/L, 0.5 g/L, and 1 g/L.

Supplementary information

Supplementary information accompanies this paper at https://doi.org/10.1186/s13068-019-1583-8.

Additional file 1. Additional Figures S1–S6 and Tables S1, S2.

Abbreviations

AAT: alcohol acetyltransferase; CBP: consolidated bioprocessing; CAT: chloramphenicol acetyltransferase; CFU: colony-forming unit; PCR: polymerase chain reactions; MSA: multiple sequence alignment; DCW: dried cell weight; DTNB: 5,5′-dithiobis-(2-nitrobenzoic acid); GC: gas chromatography; HPLC: high-performance liquid chromatography; IPTG: isopropyl β-D-1-thiogalactopyranoside; kDa: kilo Dalton; MOE: Molecular Operating Environment software; MS: mass spectrometry; OD: optical density; RMSD: root-mean-square-deviation; RT: retention time; SDS-PAGE: sodium dodecylsulfate polyacrylamide gel electrophoresis; 8-AZH: 8-azahypoxanthine; Tm: melting temperature.

Acknowledgements

The authors would like to thank the Center of Environmental Biotechnology at UTK for using the GC/MS instrument. We would also like to acknowledge the gene synthesis from The Joint Genome Institute.

Authors' contributions

CTT initiated and supervised the project. HS, JWL, and CTT designed the experiments, analyzed the data, and drafted the manuscript. HS and JWL performed the experiments. SG calculated enzyme kinetic parameters and edited the manuscript. All authors read and approved the final manuscript.

Funding

This research was financially supported in part by the NSF CAREER award (NSF#1553250) and the Center for Bioenergy Innovation (CBI), the U.S. Department of Energy (DOE) Bioenergy Research Centers funded by the Office of Biological and Environmental Research in the DOE Office of Science. The work conducted by the U.S. Department of Energy Joint Genome Institute, a DOE Office of Science User Facility, is supported by the Office of Science of the U.S. Department of Energy under Contract No. DE-AC02-05CH11231.

Availability of supporting data

One additional file contains supporting data.

Ethical approval and consent to participate

Not applicable.

Consent for publication

All the authors consent for publication.

Competing interests
The authors declare that they have no competing interests.

Author details
[1] Department of Chemical and Biomolecular Engineering, The University of Tennessee, Knoxville, TN, USA. [2] Bredesen Center for Interdisciplinary Research and Graduate Education, The University of Tennessee, Knoxville, TN, USA. [3] Center for Bioenergy Innovation (CBI), Oak Ridge National Laboratory, Oak Ridge, TN, USA.

Received: 6 June 2019 Accepted: 1 October 2019
Published online: 15 October 2019

References

1. Lange JP, Price R, Ayoub PM, Louis J, Petrus L, Clarke L, Gosselink H. Valeric biofuels: a platform of cellulosic transportation fuels. Angew Chem Int Ed Engl. 2010;49(26):4479–83.
2. Layton DS, Trinh CT. Engineering modular ester fermentative pathways in *Escherichia coli*. Metab Eng. 2014;26:77–88.
3. Layton DS, Trinh CT. Microbial synthesis of a branched-chain ester platform from organic waste carboxylates. Metab Eng Commun. 2016;3:245–51.
4. Layton DS, Trinh CT. Expanding the modular ester fermentative pathways for combinatorial biosynthesis of esters from volatile organic acids. Biotechnol Bioeng. 2016;113(8):1764–76.
5. Park YC, Shaffer CEH, Bennett GN. Microbial formation of esters. Appl Microbiol Biotechnol. 2009;85(1):13–25.
6. Tai YS, Xiong M, Zhang K. Engineered biosynthesis of medium-chain esters in *Escherichia coli*. Metab Eng. 2015;27:20–8.
7. Rodriguez GM, Tashiro Y, Atsumi S. Expanding ester biosynthesis in *Escherichia coli*. Nat Chem Biol. 2014;10(4):259–65.
8. Wilbanks B, Trinh CT. Comprehensive characterization of toxicity of fermentative metabolites on microbial growth. Biotechnol Biofuels. 2017;10(1):262.
9. Aharoni A, Keizer LC, Bouwmeester HJ, Sun Z, Alvarez-Huerta M, Verhoeven HA, Blaas J, van Houwelingen AM, De Vos RC, van der Voet H, et al. Identification of the SAAT gene involved in strawberry flavor biogenesis by use of DNA microarrays. Plant Cell. 2000;12(5):647–62.
10. Stribny J, Querol A, Perez-Torrado R. Differences in enzymatic properties of the *Saccharomyces kudriavzevii* and *Saccharomyces uvarum* alcohol acetyltransferases and their impact on aroma-active compounds production. Front Microbiol. 2016;7:897.
11. Shalit M, Katzir N, Tadmor Y, Larkov O, Burger Y, Shalekhet F, Lastochkin E, Ravid U, Amar O, Edelstein M, et al. Acetyl-coa: alcohol acetyltransferase activity and aroma formation in ripening melon fruits. J Agric Food Chem. 2001;49(2):794–9.
12. Beekwilder J, Alvarez-Huerta M, Neef E, Verstappen FW, Bouwmeester HJ, Aharoni A. Functional characterization of enzymes forming volatile esters from strawberry and banana. Plant Physiol. 2004;135(4):1865–78.
13. Urit T, Li M, Bley T, Loser C. Growth of *Kluyveromyces marxianus* and formation of ethyl acetate depending on temperature. Appl Microbiol Biotechnol. 2013;97(24):10359–71.
14. Shaw WV. Bacterial resistance to chloramphenicol. Br Med Bull. 1984;40(1):36–41.
15. Taylor MP, Esteban CD, Leak DJ. Development of a versatile shuttle vector for gene expression in *Geobacillus* spp. Plasmid. 2008;60(1):45–52.
16. Kobayashi J, Furukawa M, Ohshiro T, Suzuki H. Thermoadaptation-directed evolution of chloramphenicol acetyltransferase in an error-prone thermophile using improved procedures. Appl Microbiol Biotechnol. 2015;99(13):5563–72.
17. Groom J, Chung D, Olson DG, Lynd LR, Guss AM, Westpheling J. Promiscuous plasmid replication in thermophiles: use of a novel hyperthermophilic replicon for genetic manipulation of *Clostridium thermocellum* at its optimum growth temperature. Metab Eng Commun. 2016;3:30–8.
18. Mohr G, Hong W, Zhang J, Cui GZ, Yang YF, Cui Q, Liu YJ, Lambowitz AM. A targetron system for gene targeting in thermophiles and its application in *Clostridium thermocellum*. PLoS ONE. 2013;8(7):e69032.
19. Kannuchamy S, Mukund N, Saleena LM. Genetic engineering of *Clostridium thermocellum* DSM1313 for enhanced ethanol production. BMC Biotechnol. 2016;16(Suppl 1):34.
20. De Rossi E, Brigidi P, Welker NE, Riccardi G, Matteuzzi D. New shuttle vector for cloning in *Bacillus stearothermophilus*. Res Microbiol. 1994;145(8):579–83.
21. Rhee MS, Kim JW, Qian Y, Ingram LO, Shanmugam KT. Development of plasmid vector and electroporation condition for gene transfer in sporogenic lactic acid bacterium, *Bacillus coagulans*. Plasmid. 2007;58(1):13–22.
22. Pillai KMS. Exploring biosynthetic pathways for aromatic ester production. Master of Science. Arizona State University; 2016.
23. Zada B, Wang C, Park JB, Jeong SH, Park JE, Singh HB, Kim SW. Metabolic engineering of *Escherichia coli* for production of mixed isoprenoid alcohols and their derivatives. Biotechnol Biofuels. 2018;11:210.
24. Alonso-Gutierrez J, Chan R, Batth TS, Adams PD, Keasling JD, Petzold CJ, Lee TS. Metabolic engineering of *Escherichia coli* for limonene and perillyl alcohol production. Metab Eng. 2013;19:33–41.
25. Jang HJ, Ha BK, Zhou J, Ahn J, Yoon SH, Kim SW. Selective retinol production by modulating the composition of retinoids from metabolically engineered *E. coli*. Biotechnol Bioeng. 2015;112(8):1604–12.
26. Leslie AG, Moody PC, Shaw WV. Structure of chloramphenicol acetyltransferase at 1.75-A resolution. Proc Natl Acad Sci USA. 1988;85(12):4133–7.
27. Lynd LR, van Zyl WH, McBride JE, Laser M. Consolidated bioprocessing of cellulosic biomass: an update. Curr Opin Biotechnol. 2005;16(5):577–83.
28. Tian L, Papanek B, Olson DG, Rydzak T, Holwerda EK, Zheng T, Zhou J, Maloney M, Jiang N, Giannone RJ, et al. Simultaneous achievement of high ethanol yield and titer in *Clostridium thermocellum*. Biotechnol Biofuels. 2016;9:116.
29. Lin PP, Mi L, Morioka AH, Yoshino KM, Konishi S, Xu SC, Papanek BA, Riley LA, Guss AM, Liao JC. Consolidated bioprocessing of cellulose to isobutanol using *Clostridium thermocellum*. Metab Eng. 2015;31:44–52.
30. Thompson RA, Trinh CT. Overflow metabolism and growth cessation in *Clostridium thermocellum* DSM1313 during high cellulose loading fermentations. Biotechnol Bioeng. 2017;114(11):2592–604.
31. Holwerda EK, Thorne PG, Olson DG, Amador-Noguez D, Engle NL, Tschaplinski TJ, van Dijken JP, Lynd LR. The exometabolome of *Clostridium thermocellum* reveals overflow metabolism at high cellulose loading. Biotechnol Biofuels. 2014;7(1):155.
32. Thompson RA, Layton DS, Guss AM, Olson DG, Lynd LR, Trinh CT. Elucidating central metabolic redox obstacles hindering ethanol production in *Clostridium thermocellum*. Metab Eng. 2015;32:207–19.
33. Tyo KE, Ajikumar PK, Stephanopoulos G. Stabilized gene duplication enables long-term selection-free heterologous pathway expression. Nat Biotechnol. 2009;27(8):760–5.
34. Thompson RA, Dahal S, Garcia S, Nookaew I, Trinh CT. Exploring complex cellular phenotypes and model-guided strain design with a novel genome-scale metabolic model of *Clostridium thermocellum* DSM 1313 implementing an adjustable cellulosome. Biotechnol Biofuels. 2016;9(1):194.
35. Garcia S, Trinh CT. Multiobjective strain design: a framework for modular cell engineering. Metab Eng. 2019;51:110–20.
36. Garcia S, Trinh CT. Modular design: implementing proven engineering principles in biotechnology. Biotechnol Adv. 2019. https://doi.org/10.1016/j.biotechadv.2019.06.002.
37. Argyros DA, Tripathi SA, Barrett TF, Rogers SR, Feinberg LF, Olson DG, Foden JM, Miller BB, Lynd LR, Hogsett DA, et al. High ethanol titers from cellulose by using metabolically engineered thermophilic, anaerobic microbes. Appl Environ Microbiol. 2011;77(23):8288–94.
38. Olson DG, Lynd LR. Transformation of *Clostridium thermocellum* by electroporation. Methods Enzymol. 2012;510:317–30.
39. Kumar S, Stecher G, Tamura K. MEGA7: molecular evolutionary genetics analysis version 7.0 for bigger datasets. Mol Biol Evol. 2016;33(7):1870–4.
40. Chenna R, Sugawara H, Koike T, Lopez R, Gibson TJ, Higgins DG, Thompson JD. Multiple sequence alignment with the Clustal series of programs. Nucleic Acids Res. 2003;31(13):3497–500.
41. Robert X, Gouet P. Deciphering key features in protein structures with the new ENDscript server. Nucleic Acids Res. 2014;42(Web Server issue):W320–4.

42. Biswas T, Houghton JL, Garneau-Tsodikova S, Tsodikov OV. The structural basis for substrate versatility of chloramphenicol acetyltransferase CATI. Protein Sci. 2012;21(4):520–30.
43. Leslie AG. Refined crystal structure of type III chloramphenicol acetyltransferase at 1.75 A resolution. J Mol Biol. 1990;213(1):167–86.
44. Beaman TW, Sugantino M, Roderick SL. Structure of the hexapeptide xenobiotic acetyltransferase from *Pseudomonas aeruginosa*. Biochemistry. 1998;37(19):6689–96.
45. Bordoli L, Kiefer F, Arnold K, Benkert P, Battey J, Schwede T. Protein structure homology modeling using SWISS-MODEL workspace. Nat Protoc. 2009;4(1):1–13.
46. Day PJ, Shaw WV, Gibbs MR, Leslie AG. Acetyl coenzyme A binding by chloramphenicol acetyltransferase: long-range electrostatic determinants of coenzyme A recognition. Biochemistry. 1992;31(17):4198–205.
47. Lee JW, Niraula NP, Trinh CT. Harnessing a P450 fatty acid decarboxylase from *Macrococcus caseolyticus* for microbial biosynthesis of odd chain terminal alkenes. Metab Eng Commun. 2018;7:e00076.
48. Lewendon A, Murray IA, Shaw WV, Gibbs MR, Leslie AG. Evidence for transition-state stabilization by serine-148 in the catalytic mechanism of chloramphenicol acetyltransferase. Biochemistry. 1990;29(8):2075–80.
49. Gibson DG. Enzymatic assembly of overlapping DNA fragments. Methods Enzymol. 2011;498:349–61.
50. Zheng L, Baumann U, Reymond JL. An efficient one-step site-directed and site-saturation mutagenesis protocol. Nucleic Acids Res. 2004;32(14):e115.
51. Green MR, Sambrook J. Molecular cloning., A laboratory manualCold Spring Harbor: Cold Spring Harbor Laboratory Press; 2001.
52. Guss AM, Olson DG, Caiazza NC, Lynd LR. Dcm methylation is detrimental to plasmid transformation in *Clostridium thermocellum*. Biotechnol Biofuels. 2012;5(1):30.
53. Lee J-W, Trinh CT. Microbial biosynthesis of lactate esters. Biotechnol Biofuels. 2019;12(1):226.
54. Bradford MM. A rapid and sensitive method for the quantitation of microgram quantities of protein utilizing the principle of protein-dye binding. Anal Biochem. 1976;72:248–54.
55. Lo MC, Aulabaugh A, Jin G, Cowling R, Bard J, Malamas M, Ellestad G. Evaluation of fluorescence-based thermal shift assays for hit identification in drug discovery. Anal Biochem. 2004;332(1):153–9.
56. Ellman GL. Tissue sulfhydryl groups. Arch Biochem Biophys. 1959;82(1):70–7.
57. Jones E, Oliphant T, Peterson P et al. SciPy: open source scientific tools for Python. 2019. https://docs.scipy.org/doc/scipy/reference/generated/scipy.optimize.curve_fit.html. Accessed 4 Feb 2019.
58. Mayorov N. Robust non linear regression in SciPy. 2019. https://scipy-cookbook.readthedocs.io/items/robust_regression.html. Accessed 4 Feb 2019.
59. Marasovic M, Marasovic T, Milos M. Robust nonlinear regression in enzyme kinetic parameters estimation. J Chem-Ny. 2017. https://doi.org/10.1155/2017/6560983.
60. Dubois M, Gilles K, Hamilton JK, Rebers PA, Smith F. A colorimetric method for the determination of sugars. Nature. 1951;168(4265):167.

Publisher's Note